G3: Genes|Genomes|Genetics Early Online, published on December 30, 2016 as doi:10.1534/g3.116.036459

Comparative high-density linkage mapping reveals conserved genome structure but variation in levels of heterochiasmy and location of recombination cold spots in the common frog

Gemma Palomar[*†], Freed Ahmad[‡], Anti Vasemägi[‡§], Chikako Matsuba[*†], Alfredo G. Nicieza[*†] and José Manuel Cano[*†]

[*] Research Unit of Biodiversity (UO-CSIC-PA), 33600 Mieres, Asturias, Spain.
[†] Department of Biology of Organisms and Systems, University of Oviedo, 33006 Oviedo, Asturias, Spain.
[‡] Department of Biology, University of Turku, 20014 Turku, Finland.
[§] Department of Aquaculture, Institute of Veterinary Medicine and Animal Science, Estonian University of Life Sciences, 51006 Tartu, Estonia.

Draft genome is available at https://figshare.com/s/c0ff6bacbfc4572e1ff1 and marker sequences are available at https://figshare.com/s/24fa6c7cd2f133467207

Running title: Spanish *R. temporaria* linkage map.

Key words: Linkage map, *Rana temporaria*, Spanish lineages, recombination cold spots, heterochiasmy.

Corresponding author: Gemma Palomar.
Address: Research Unit of Biodiversity (UO-CSIC-PA), Edificio de Investigación, Gonzalo Gutiérrez Quirós s/n, 33600, Mieres, Asturias, Spain.
Phone: 0034 985103000 (ext.5935).
Email: gemma.palomar@yahoo.es

ABSTRACT

By combining 7077 SNPs and 61 microsatellites, we present the first linkage map for some of the early diverged lineages of the common frog, *Rana temporaria,* and the densest linkage map to date for this species. We found high homology with the published linkage maps of the Eastern and Western lineages but with differences in the order of some markers. Homology was also strong with the genome of the Tibetan frog *Nanorana parkeri* and we found high synteny with the clawed frog *Xenopus tropicalis*. We confirmed marked heterochiasmy between sexes and detected non-recombining regions in several groups of the male linkage map. Contrary to the expectations set by the male heterogamety of the common frog, we did not find male heterozygosity excess in the chromosome previously shown to be linked to sex determination. Finally, we found blocks of loci showing strong transmission ratio distortion. These distorted genomic regions might be related to genetic incompatibilities between the parental populations, and are promising candidates for further investigation into the genetic basis of speciation and adaptation in the common frog.

INTRODUCTION

Intra and interspecific comparative genomic studies shed light on basic evolutionary processes such as sexual differentiation, adaptation, and speciation (Koonin *et al.* 2000; Kocher 2004; Nadeau and Jiggins 2010; Bachtrog 2013). While comparative genomic studies have mostly focused on model organisms, such as humans and mice (e.g. Bernstein *et al.* 2005), the advances in next

58 generation sequencing technology have facilitated genomic analysis in species
59 lacking a reference genome (Kocher 2004; Miller *et al.* 2007; Gagnaire *et al.*
60 2013; Brelsford *et al.* 2016a). Amphibians are good models for comparative
61 genomics due to their extraordinary biodiversity, worldwide distribution, and
62 wide range of variation in genome size and karyotype (Duellman and Trueb
63 1986; Green and Sessions 1991). In particular, the common frog, *Rana*
64 *temporaria*, has a wide distribution range across contrasting environmental
65 conditions and very well reported cases of local adaptation (Miaud *et al.* 1999;
66 Laurila *et al.* 2002; Laugen *et al.* 2003; Cano *et al.* 2004; Phillimore *et al.* 2010).
67 Phylogenetic analyses of the common frog have revealed multiple, deeply
68 diverged evolutionary lineages or clades across Europe (Palo *et al.* 2004; Vences
69 *et al.* 2013). There are two widely distributed, Western and Eastern clades, that
70 separated ca. 0.7 My ago (Palo *et al.* 2004) and whose contact zone is in Central
71 Europe (Schmeller *et al.* 2008; Teacher *et al.* 2009; Vences *et al.* 2013). In
72 northwest Spain, another divergent evolutionary lineage, frequently referred to
73 as subspecies *R. t. parvipalmata* (Seoane 1885), has been identified. This lineage
74 is basal (i.e. divergence 1.12 Ma ago) to the Western and Eastern clades (Veith *et*
75 *al.* 2002; Veith *et al.* 2003; Palo *et al.* 2004). In addition, there is evidence for at
76 least one other lineage, a sister group of *R. t. parvipalmata*, also located in
77 northern Spain (Vences *et al.* 2013).
78 Earlier linkage maps of *R. temporaria* have been constructed using individuals
79 from the Western and Eastern clades (Cano *et al.* 2011; Rodrigues *et al.* 2013;
80 Rodrigues *et al.* 2016). The Western and Eastern lineage maps showed different
81 locus order that might indicate potential genomic rearrangements (e.g. in linkage
82 groups Xt3, Xt5, Xt6 and Xt7B) which might be linked to adaptive processes (Lee

2002). However, we still lack a comprehensive understanding of the genomic differences among lineages of the common frog, and especially about the genome structure of the early diverged lineages in the north of the Iberian Peninsula. The aim of the present study is to compare recombination patterns, synteny, and putative sex-linked chromosomes of the Iberian lineages with more recently diverged lineages of the common frog. To accomplish these objectives, we used *Restriction site-Associated DNA* (RAD) sequencing and microsatellite markers to construct a high-density consensus linkage map of *R. temporaria* based on a cross between parents from the southwestern end of the species range in the north of the Iberian Peninsula.

MATERIAL AND METHODS

Mapping family and DNA extraction

This study is based on a large full-sib family from a single *R. temporaria* cross. Adults were sampled in two localities from the North of Spain (Bárcena Mayor, Cantabria, N 43.13103 W 4.17879; and Vega de Candioches, León, N 42.99910 W 5.92124). We crossed a male from Candioches (high altitude: 1687 m.a.s.l.) and a female from Bárcena (low altitude: 551 m.a.s.l.) belonging to two different mtDNA clades (Vences *et al.* 2013; Nicieza A.G. unpublished data). Frogs from these localities are exposed to contrasting environmental conditions (i.e. highland with short growing season and cold winters vs. lowland with long growing season and mild winters). The controlled cross was carried out in the laboratory of the Amphibian Facilities at the University of Oviedo. Female and male abdomens were pressed gently by hand to obtain eggs and sperm without

harming the animals. Tadpoles were individualized at Gosner stage 25 and were kept at 12h light-12h dark photoperiod and 14ºC until reached Gosner stage 42. Then, they were euthanized with an overdose of benzocaine and frozen. DNA from brain of parents and 184 F1 offspring was extracted with the DNeasy Blood and Tissue Kit (Qiagen). DNA quality was assessed using 0.7% agarose gel electrophoresis and DNA concentration was determined with Qubit® fluorometer. DNA extractions were diluted to 100 ng/µl for subsequent library preparation.

Restriction site-associated DNA sequencing (RAD-seq)

Two libraries were prepared according to slightly modified Elshire et al. (2011) protocol (File S1). Briefly, DNA was digested with restriction enzymes *Pst*I and *Bam*HI and the fragments of each individual were ligated to one of the 94 modified Illumina adapters, which contain barcode sequences, with T4 DNA ligase. Adapter-ligated DNA was combined to two library pools consisting of 92 offspring and the two parents in each pool. After purification, DNA fragments of a certain size (300-600 bp range) were selected in each library using an E-Gel® iBase™ Power System as in Pukk et al. (2015). Size selected fragments were amplified by a PCR using 18 cycles and purified with QIAquick PCR purification kit (QIAGEN). Agilent 2100 Bioanalyzer system was used to check the quality and quantity of size selected and amplified libraries. At the end, fragments of average 400bp length (80% of fragments with size range 300-550bp) from the two libraries were sequenced on two paired ends lanes (2x100) with the Illumina HiSeq 2000 in the Illumina Genome Analyzer platform at the Center for Genomic Regulation in Barcelona, Spain.

Genotyping

Raw Illumina reads with low quality were discarded as well as reads with ambiguous barcode sequences. As the forward and reverse reads did not overlap, forward reads were used for the first part of the analysis. We demultiplexed the sequences and barcodes were trimmed as a result of this process. Low quality ends were discarded resulting in 91 bp reads. Because of the lack of a reference genome of *R. temporaria*, the reads from the presumably heterogametic parent (i.e. sire) were used to generate the reference sequence. To that end, firstly, identical reads were collapsed with FASTQ/A Collapser of the FASTX-toolkit (Gordon and Hannon 2010). Secondly, the remaining sire's sequences were clustered with CD-HIT EST (Li 2015) at 90% of similarity. An assembly *de novo* was performed with the resulting contigs in the MIRA assembler (Chevreux 2007) and a sire-based reference sequence was obtained for each contig. Thirdly, the reads of the dam and sire were aligned to this reference sequence using the software Bowtie2 (Langmead and Salzberg 2012). The dataset of forward read contigs was obtained after discarding contigs mapped with less than 10 reads or more than 1000 reads for each parent as well as those with more than 10% of mismatch. We used the information from the forward read to select the corresponding reverse read and create a dataset for both forward and reverse read contigs. Fourthly, to select informative loci, we conducted parental SNP calling with the software Samtools (Li *et al.* 2009). A heterozygotic genotype was called when the minor allele frequency (MAF) among reads was >0.1. Uninformative SNPs (i.e. both parents with alternative homozygous genotypes) were discarded. Finally, the selected SNPs were used to

158 map the progeny reads. Following DaCosta and Sorenson (2014) and minimizing
159 the mismatching, contigs mapped with less than 200 or more than 20,000 total
160 reads were rejected.
161 SNP-calling was performed again with a quality threshold of 100 and a maximum
162 of four SNPs allowed per contig. Parents and progeny were deemed
163 heterozygotes if the MAF was >0.1 and SNPs were excluded if more than 25% of
164 progeny genotypes were missing and more than 6% of progeny showed non-
165 compatible genotypes. SNPs showing segregation distortion were not included in
166 the initial linkage maps (X^2 test, $p<0.05$). However, later, for determining
167 potentially incompatible regions between the two lineages, we retained loci
168 showing relatively mild segregation distortion (X^2 test, p-value 0.05-0.005) for
169 construction of new linkage maps and permutation analysis (see Transmission
170 ratio distortion section). Genotyping error was calculated for both sire and dam
171 by comparing replicated genotype calls obtained from two separate sequencing
172 lanes.
173
174 **Microsatellites**
175 In addition to the SNPs, microsatellite markers were also included to enable
176 direct comparison with the previous maps (Cano *et al.* 2011; Rodrigues *et al.*
177 2013). From 116 tested markers (File S3), 113 microsatellites were successfully
178 amplified within 19 multiplex reactions following the protocol of the QIAGEN®
179 Multiplex PCR Master Mix (2X) at half volume (25 µl). Amplification reactions
180 started with an initial polymerase activation step at 95 °C for 15 min, followed by
181 40 cycles of: 94 °C for 30 s, 55 °C (for the markers: Rib01, Rib 06, Rib 08, and
182 Rib15) or 60°C (for the rest) for 90 s, and 72 °C for 60 s; and finally, an extension

183 stage of 60 °C for 30 min. Microsatellite analysis was performed using an ABI
184 3100 automatic DNA Sequencer.
185 Genotypes were determined using the software GENEMARKER v 2.4 (Soft
186 Genetics, State College, PA, USA). Uninformative microsatellites, as well as those
187 with null alleles, were excluded from subsequent analysis (File S3).
188 As the SNPs from the RAD-sequencing, microsatellites showing Mendelian
189 segregation violations (X^2 test, $p<0.05$) were removed before the linkage
190 analysis.
191
192 **Map construction**
193 Markers, both SNPs and microsatellites, were assigned according to their
194 segregation pattern to five categories: *nn*x*np*, *lm*x*ll, ef*x*eg*, *abxcd,* and *hk*x*hk*. Sex-
195 specific maps were constructed from informative markers of each sex (*nn*x*np*
196 and *lm*x*ll*) using the cross type "doubled haploid" (DH) and Maximum Likelihood
197 algorithm in MSTmap (Wu *et al.* 2008). This algorithm has shown to be more
198 successful at ordering the loci compared to other methods, such as weighted
199 least squares and minimum sum of adjacent recombination fractions (Hackett
200 and Broadfoot 2003). The Kosambi mapping function was used to calculate the
201 genetic distance between markers and a p-value of $1x10^{-8}$ was used as threshold
202 for clustering the markers into the linkage groups. Due to the lack of linkage
203 phase information, the dataset was duplicated, changing the phase of each
204 marker (Gadau *et al.* 2001; Brelsford *et al.* 2016a). Duplicated linkage groups
205 were eliminated manually in the output. As a conservative approach, we used the
206 option '*detect bad data*' in the software. In addition, possible double cross-overs

were transformed to unknown (U) iteratively followed by an additional round of linkage map reconstruction, until no possible double cross-over was found. The average linkage map was created using the option appropriate for an outbred full-sib family (cross pollinator, CP) in Joinmap 4.1 (Van Ooijen 2011). Identical loci were excluded to decrease computational time and added again after map construction. Linkage groups were identified with a LOD threshold of eight. Small linkage groups (i.e. less than four markers) were excluded from further analysis. The order of the markers within each linkage group was determined with the Maximum Likelihood mapping algorithm, which assumes no crossover interference. Therefore, the distance between markers was calculated using the Haldane mapping function. Spatial sampling was used with five thresholds: 0.1, 0.05, 0.03, 0.02, and 0.01. Three map optimization rounds were run in each spatial sample, using the following parameters: chain length was 10,000, cooling control parameter was 0.0001, and the rounds were stopped after 100,000 chains without improvement. Finally, for the multipoint estimation of recombination frequencies, we used a burn-in of 100,000, five cycles of Monte Carlo Expectation Maximization (chain length per cycle: 100,000), and six sampling periods for recombination frequency. Stabilization of the recombination frequencies was monitored with the sum of recombination frequencies of adjacent fragments and the mean number of recombination. The name of the linkage groups follows the *Xenopus tropicalis* homology. The expected genome length and observed genome coverage were calculated according to Chakravarti et al. (1991) and Cervera et al. (2001) respectively. The observed length (G_O) was the sum of the observed length of the linkage groups. The expected length (G_E) was the sum of the expected length of the linkage

groups, which was calculated multiplying the observed length of each linkage group by the factor (m + 1)/(m - 1), being m the number of markers of the linkage group. The observed genome coverage, understood as the proportion of the genome comprised in our recombination map, was the ratio G_O/G_E.

Transmission ratio distortion markers

Earlier studies have demonstrated that excluding markers that show segregation distortion from linkage mapping may result in the exclusion of certain chromosome regions from the map (Cervera *et al.* 2001; Doucleff *et al.* 2004). However, a large number of distorted markers may also increase the chance of type I errors and may result in inaccurate estimation of genetic distances (Cervera *et al.* 2001). Therefore, we included only markers with moderate levels of segregation distortion (X^2 p-values from 0.05 to 0.005) in the linkage analysis. None of the markers caused big gaps (i.e. >50cM) of recombination distance. To identify distorted regions, instead of only distorted markers, we used a kernel smoothing and permutation test (for details see Bruneaux *et al.* 2013; Ozerov *et al.* 2016). By taking into account differences in marker density, this strategy increases the statistical power for detecting regions where several adjacent markers show high distortion. For this analysis, we ran one million permutations in the R software v. 3.0.2 (R Core Team 2013).

Analysis of the homology

The genomes from *Xenopus tropicalis* (version 9.0, xenbase.org) and *Nanorana parkeri* (version 2, gigadb.org) were used to evaluate the homology and the synteny among amphibian genomes. References from both forward and reverse

sire contigs containing SNPs of the linkage map were aligned to a draft genome of *R. temporaria* (File S2) using Bowtie2 (Langmead and Salzberg 2012). The draft scaffolds were selected when forward and reverse references aligned within 600bp from each other because, during library construction, the size of the fragments was shorter than 550bp. This allowed the use of longer sequences for inter-specific comparisons, increasing the power of the homology searches. We searched for homology in NCBI Nucleotide (ncbi.nlm.nih.gov) and Swissprot (uniprot.org) databases as well as in *Xenopus tropicalis* and *Nanorana parkeri* genomes using blast. Homologous sequences of other species were retained if the best hit e-value was five orders of magnitude higher than the second best hit e-value (Brelsford *et al.* 2016a; Brelsford *et al.* 2016b). To visualize the synteny between *R. temporaria* and *X. tropicalis*, we used the software Circos plot v 0.69-2 (Krzywinski *et al.* 2009) as in Yang et al (2014).

Data availability

File S1 contains a detailed protocol of the library preparation. File S2 contains the pipeline for the construction of the draft genome. File S3 contains detailed information about the microsatellites used (i.e. accession numbers, core motifs and references). File S4 contains sex specific and average maps and a comparison with previous microsatellite maps. File S5 contains supplementary figures and tables being: Figure S1, linear model that fits the relation between male and female number of markers; Figure S2, linkage group specific male vs. female recombination lengths; Figure S3, map length and number of markers compared to Swiss map; Figure S4, kernel smoothing results; Table S1, summary of distorted maps, linkage group lengths, number of markers and sex specific

recombination rates. File S6 contains a figure of the distorted sex specific map. File S7 contains sex specific distorted maps and the results of the kernel analysis. File S8 contains the genotypic information of the individuals. Draft genome is available at https://figshare.com/s/c0ff6bacbfc4572e1ff1 and marker sequences are available at https://figshare.com/s/24fa6c7cd2f133467207.

RESULTS

Microsatellite and RAD analysis

Out of the 113 amplified microsatellites, 77 were heterozygous at least in one parent. Twelve of them possessed null alleles and four loci showed Mendelian segregation violation (p-value < 0.0001), resulting in a final set of 61 informative microsatellites (File S3). In the whole dataset, 19 offspring exhibited three alleles at least in one microsatellite locus, suggesting potential partial trisomy, and were excluded from subsequent analysis.

A total of 162 F1 offspring were used to construct the linkage map, after discarding three individuals with less than 5,000 reads. Approximately 634 million reads were retained after the quality filtering. Over 10 million reads were obtained from each parent, while on average 3.8 million of reads were sequenced per offspring (ranging from 2 to 6.8 million). The assembly from the parental read alignment resulted in 88,497 contigs. From those, 13,203 contigs were polymorphic and were used for mapping the reads from the progeny and SNP calling. Over 13,600 SNPs were initially identified from which 7,217 markers passed X^2 test for Mendelian segregation (p-value > 0.05). The

306 estimated genotyping error inferred based on independent technical replicates
307 was around 5% (5.5% sire and 5.3% dam).
308 Sex-specific linkage maps were constructed using 3,644 markers (51
309 microsatellites and 3593 SNPs) and 3,180 markers (51 microsatellites and 3129
310 SNPs), for female and male respectively. After discarding linkage groups formed
311 by less than four markers, 13 linkage groups were recovered in both maps
312 (Table 1). A total of 3,596 markers in the female map and 3,105 markers in the
313 male map were assigned to the 13 linkage groups (File S4). Our map presented
314 an observed genome coverage of 99% for both sexes. The average recombination
315 rate was 1.35 times higher and the total length was roughly two-fold (1.87 times)
316 larger in the female map than in the male map. Interestingly, all male linkage
317 groups contained a cluster of markers with zero recombination, henceforth
318 recombination cold spot (Figure 1). The number of clustered non-recombining
319 markers was higher in the largest linkage groups (i.e. Rt1, Rt2, Rt3, Rt5, and Rt6)
320 ranging from 86 to 159 markers, while 9 to 62 non-recombining markers were
321 detected in smaller linkage groups in the male map. The non-recombining
322 regions in the female map were generally smaller (<23 markers). However, the
323 linkage groups Rt4B, Rt7B, and Rt10 showed non-recombining regions of similar
324 length in both sexes (Table 1).
325 Our results showed that the linkage group Rt1 is the longest and contains the
326 largest number of markers in both sexes (Figures 1 and 2). The female map
327 presented a slightly higher number of markers per linkage group, except for -
328 Rt4A and Rt6 (Table 1). Rt6 deviated from the general trend due to a larger
329 number of markers in the male than in the female map (Figure 2; Figure S1).
330 Furthermore, female map showed higher recombination length than male map

but some linkage groups deviated above or below from the general trend (Figure S2). For instance, Rt6 was longer in the male map and Rt10 was shorter in the female map compared to other linkage groups. Rt3 exhibited the lowest recombination rate in the male map. Finally, Rt7B was the shortest linkage group in the male map with the smallest number of markers (Table 1).

Compared with the recent RAD-based linkage map in the common frog (Brelsford *et al.* 2016b), the number of markers and recombination length of the linkage groups in our study was similar (coefficient of determination, female map length R^2=0.83, number of markers in female map R^2=0.92, number of markers in male map R^2=0.90, all p-values<0.05) except for the length of the male linkage groups (coefficient of determination, R^2=0.09, p-value>0.05) (Figure S3). The lack of correlation between length of male linkage groups and number of markers supports the independence between number of crossovers and chromosome size in males.

Transmission ratio distortion

In order to evaluate the segregation distortion patterns along the chromosomes, 521 and 401 distorted markers of dam and sire, respectively, were added to construct new sex-specific maps. Among the distorted markers, a total of 500 SNPs segregating in the dam (12.2% of total number of markers) and 375 SNPs segregating in the sire (10.8% of total number of markers) were successfully assigned within the 13 linkage groups (File S7). The resulting map was 663 cM longer in the female and 398 cM longer in the male compared to the maps without including distorted markers. Average recombination rate was similar in distorted and non-distorted maps (Table S1). The distribution of the distorted

markers exhibited a non-uniform pattern along and among linkage groups (File S6). For example, a large number of distorted markers was observed on Rt1 in contrast with the low number on Rt4B and Rt7A. Furthermore, there were differences between sexes. Kernel smoothing results showed a higher distortion in the female than in the male map (Figure S4). Only Rt2, Rt5, Rt7B, Rt8B, and, Rt9 from male map exhibited regions with signals of high distortion based on the kernel analysis while all female linkage groups, except Rt9, contained at least one area with excess of distorted markers. Interestingly, Rt6 and Rt9 from the male map and Rt7B from the female map showed clusters of distorted markers within the recombination cold spots (Figure 3).

Average map

We used 7278 markers (61 microsatellites and 7217 SNPs) to construct the average linkage map and 7138 markers were successfully assigned to 13 linkage groups. All the linkage groups reached stabilization after five Monte Carlo Expectation Maximization cycles. All markers were located within the same linkage groups as in sex-separated maps. However, as expected, the average map showed less accurate marker order than the female map.

Similarity analysis

A total of 4161 forward and reverse reference sequences from the sire were aligned to the *R. temporaria* draft genome. In 2359 cases (56.7%) the pair of forward and reverse reference sequences aligned onto the same scaffold within 600bp (range from 190 to 473 bp). From a total of 2331 scaffolds selected, 1184 aligned to the *N. parkeri* genome (50.8%) and 305 aligned to the *X. tropicalis*

genome (13%). In addition, 81% of homologous sequences between *R. temporaria* and *X. tropicalis* were located in the same chromosome and the synteny was also strong as is shown in the Circos plot (Figure 3).

DISCUSSION

We have generated the densest linkage map for the common frog to date. The combined use of SNPs and microsatellites allowed in-depth comparison with the existing linkage maps for the species allowing, for the first time, a detailed analysis of the early diverged Iberian lineages in relation to the, more recently diverged, Western and Eastern lineages.

Both the number and relative length of our linkage groups matched the karyotype described for the species, with five large and eight short chromosomes (Spasić-Bošković *et al.* 1997). Furthermore, we observed a strong synteny between the *R. temporaria* linkage map and the genome of *X. tropicalis*. Heterochiasmy was pronounced, with a lower recombination rate in the male map. Finally, some regions exhibited a strong transmission ratio distortion which might be indicative of genetic incompatibilities between the lineages used in our experimental cross. Below we discuss in detail the recombination patterns and evolutionary processes that may have shaped the differences found among the lineages of *Rana temporaria*.

Comparison with previous microsatellite maps

405 The obtained consensus linkage map was consistent with previous microsatellite
406 maps based on the Western and Eastern lineages (Cano *et al.* 2011; Rodrigues *et*
407 *al.* 2013; Rodrigues *et al.* 2016). However, compared to the first linkage map
408 based on Swedish populations from the Eastern lineage (Cano *et al.* 2011), our
409 map revealed several differences. For example, markers that showed significant
410 linkage in groups 1, 4, and 12 from Cano et al. (2011) were unlinked in our map
411 and located in other linkage groups (File S4). On the other hand, linkage groups
412 15 and 2 from Cano et al. (2011) were joined within the largest group, Rt1, in our
413 map (File S4). Separation of these two linkage groups in Cano et al. (2011) was
414 likely due to lower coverage. Since Rodrigues *et al*. (2016) also found similar
415 inconsistencies in their map based on Swedish populations, the observed
416 discrepancies are may be caused by differences in coverage and methodology.
417 Nevertheless, our results revealed frequent change in marker order compared to
418 the published maps (File S4), hence, further research is needed to determine if
419 some of these changes can reflect the occurrence of independent chromosomal
420 rearrangements, such as inversions, among the different lineages.
421
422 **Recombination rate**
423 Similar to earlier studies, we detected large differences in recombination rate
424 between sexes (Berset-Brändli *et al.* 2008; Cano *et al.* 2011; Rodrigues *et al.*
425 2013; Brelsford *et al.* 2016b). The average recombination rate was 1.36 times
426 larger in the female than in the male map. This heterochiasmy is smaller than
427 that observed in maps from the Eastern (1.76 times; Cano *et al.* 2011) and
428 Western lineages, both based solely on microsatellite markers (82.5 times;
429 Rodrigues *et al.* 2013) and SNPs (3.15 times; Brelsford *et al.* 2016b). In relation

to the total length of the maps, our female map was 1.87 times larger than the male map, similar to the first Eastern clade map (1.52 times, Cano *et al.* 2011) but more discordant with the second Eastern clade map (17.4 times, Rodrigues *et al.* 2016) and the Western clade maps, which ranged from 3.37 to 72 times (Rodrigues *et al.* 2013; Brelsford *et al.* 2016b). All in all, the heterochiasmy pattern observed in this study was similar to the first Eastern lineage map (Cano *et al.* 2011) which was also based on an outcross. More families from the North Iberian lineages would be needed to confirm these findings.

Concerning the sex-specific recombination patterns, female recombination rates were fairly constant overall while male recombination rates were reduced in the majority of the linkage groups (Figure 1). Similar to Brelsford et al. (2016b), a cluster of markers with no recombination occurred in every chromosome, forming an extensive suppressed-recombination region in the largest linkage groups. In amphibians, male recombination is usually restricted to telomeric areas and the non-recombining region is near the center of the linkage group (Morescalchi and Galgano 1973), coinciding with the centromere and paracentromere area (King 1991). This pattern was found in *Hyla arborea* (Brelsford *et al.* 2016a) and it is in accordance with the metacentric/submetacentric chromosomes described in the karyotype of *R. temporaria* based on populations from the Eastern lineage (Spasić-Bošković *et al.* 1997). However, the position of the non-recombining regions in our map was shifted to one side in Rt1, Rt2, and Rt3 (Figure 1). Furthermore, subtelomeric/telomeric recombination cold spots were also observed in some linkage groups of the Western clade (Figure 1 from Brelsford *et al.* 2016b). The

authors suggested that the shifted position in their map could be the lack of coverage at the chromosome ends (Brelsford pers.comm.). However, because of the higher coverage of the current map and the good homology with the terminal regions of the chromosomes in *X. tropicalis*, the map presented here reflects well the actual position of the recombination cold spots in the chromosomes. Hence, our results call for further karyotype and whole genome sequencing work between the Iberian and more recently diverged lineages to establish whether centromere repositioning has occurred in the species.

The Iberian Peninsula has been suggested as the place where *R. temporaria* originated (Vences *et al.* 2013) and the Northwest Iberian lineages diverged 1.12 My ago from the lineage for which the karyotype of the species was described (i.e. Balkans), being isolated in different refugia during the last glaciation. Centromere repositioning events have been observed at similar evolutionary time scales but only at the interspecific level. For example, five centromere repositioning events have occurred between donkeys and zebras, which diverged from each other 1-2.78 My ago (Carbone *et al.* 2006; Vilstrup *et al.* 2013).

Putative sex linkage group

R. temporaria, as is the case in other *Rana* species, exhibits male heterogamety (XY). If sex determination is strictly genetic, and there is no recombination between sex-chromosomes, X and Y are expected to accumulate differences as a result of large rearrangements and/or degeneration of the Y chromosome (Charlesworth and Charlesworth 2000; Charlesworth *et al.* 2005). Thus, over time, heterogamety is expected to result in an excess of heterozygotes in the

480 linkage group(s) containing the sex determining gene(s). Based on this
481 expectation, and evidence in *Hyla arborea* frogs, Brelsford et al. (2016a)
482 proposed a method to detect sex chromosomes based solely on heterozygosity
483 differences among linkage groups.
484 Nevertheless, X and Y chromosomes are homomorphic in the common frog and
485 recombination between them still seems to occur as reported for other
486 amphibian species (Stöck *et al.* 2013; Dufresnes *et al.* 2014). Perrin (2009)
487 suggested that occasional sex-reversal events could maintain X-Y recombination
488 because XY females would prevent the decay of the Y chromosome. In fact,
489 spontaneous sex-reversed individuals, including observed XX males and possibly
490 XY females, have been documented in some populations (Matsuba *et al.* 2008;
491 Perrin 2009; Alho *et al.* 2010). Previous studies found several sex-linked
492 markers in the linkage group Rt1 and it has been considered as the putative sex
493 chromosome for the species (e.g. Matsuba *et al.* 2008; Alho *et al.* 2010; Cano *et al.*
494 2011; Rodrigues *et al.* 2013). However, both Brelsford et al. (2016) and our
495 study failed to find the expected heterozygosity excess in Rt1 as putative sex
496 chromosome. Since we lacked phenotypic sex information for our family, we
497 cannot establish whether non-genetic sex determination plays a role in our
498 results, although this was the case in Brelsford et al. (2016).
499 On the other hand, Rt6 showed marked higher male heterozygosity in our cross
500 (Figure 2; Figure S1) and harbored two sex-linked markers in the Finnish
501 population of Kilpisjärvi (BFG267 and BFG239, Matsuba unpublished data).
502 Therefore, this linkage group warrants further research to determine its
503 potential involvement in sex determination or whether another source of
504 differentiation among the lineages crossed is causing this large male

heterozygosity. The possibility of multiple chromosomes participating in the sex determination of the common frog has also been discussed in previous work (Cano *et al.* 2011; Rodrigues *et al.* 2013; Rodrigues *et al.* 2014) and demonstrated recently by Rodrigues *et al.* (2016). Alternatively, a large autosomal supergene with two differentiated haplogroups in the crossed lineages could also produce higher male heterozygosity, if the male were heterozygous and the female were homozygous (Brelsford *et al.* 2016a).

Segregation distortion

Many biological processes acting before or after fertilization can cause transmission ratio distortion (Fishman *et al.* 2001; Kuittinen *et al.* 2004). We found clusters of distorted markers in the non-recombining regions of the linkage groups Rt6 and Rt9 in the male and Rt7B in the female, based on the randomization and kernel smoothing approach. There are non-genetic sources of segregation distortion such as genotyping errors, sampling biases, and comigration (Rogers *et al.* 2007; Zhou *et al.* 2015). Our genotyping-by-sequencing dataset contained around 5% of genotyping errors based on analysis of replicated samples, despite the rather strict quality control. However, such technical artifacts are not expected to systematically cluster together in relation to other loci. Thus, the distorted genomic regions with blocks of distorted markers found in this study are likely related to biological processes such as meiotic drive, lineage incompatibilities, or outbreeding depression (Zhou *et al.* 2015). Since we observed high mortality and deformity rate in our experiment, these genomic regions are good candidates to investigate potential genetic incompatibilities. Furthermore, loci with non-Mendelian inheritance could have

530 greater evolutionary importance than their current knowledge suggests (Lyttle
531 1991; Taylor and Ingvarsson 2003). However, analysis of gametes and replicate
532 families generated preferably using backcross breeding design would be needed
533 to further understand the relationship between genome structure and
534 segregation distortion.
535
536 **Homology analysis**
537 The comparative genomic analysis between *R. temporaria, X. tropicalis* and *N.*
538 *parkeri* supported the strong homology among amphibian genomes (Brelsford *et*
539 *al.* 2013; Brelsford *et al.* 2016a). As expected from their close phylogenetic
540 relationship (Pyron and Wiens 2011), *N. parkeri* showed higher homology with
541 *R. temporaria*. These species diverged 90 My ago while *X. tropicalis* and *R.*
542 *temporaria* split approximately 208 My ago (divergence times retrieved from
543 timetree.org). The estimated homology between *R. temporaria* and *X. tropicalis* in
544 this study (12.8%) is slightly higher than the observed (10%) for the Western
545 lineage of this species (Brelsford *et al.* 2016b). Our study confirmed the finding
546 of Brelsford et al. (2016b), that *X. tropicalis* chromosomes 4, 7, and 8 were split
547 into two pairs in *R. temporaria*.
548
549 **Conclusions**
550 The constructed high-density consensus linkage map provides an important
551 resource for further research in the evolutionary biology of *R. temporaria*,
552 facilitating the search for genes of adaptive relevance. In addition, due to the
553 conserved synteny among amphibians, this linkage map represents a valuable
554 tool for further comparative genomic studies. Our work indicates that the

555 genome structure is generally conserved between common frog lineages while
556 the position of the recombination cold spots and marker order can vary. Finally,
557 genomic regions showing strong transmission distortion found here are
558 promising candidates for studying incipient speciation processes.
559
560 **Acknowledgements**
561 We would like to thank Cristina García for help in fieldwork and tadpole care and
562 Leticia Viesca for help with laboratory tasks. We are indebted to Luming Yang
563 who kindly shared his Circos plot script with us. We would also like to thank
564 Alan Brelsford for assistance with data analysis and interpretation and Nicolas
565 Perrin for providing additional details about their published work. We are
566 grateful to John Loehr for improving English grammar. Our research was
567 supported by the following grants: Spanish Ministry of Education (reference
568 CGL2011-23443), Ministry of Economy and Competitiveness (reference BES-
569 2012-055220), National Parks Autonomous Agency (OAPN) (reference MARM
570 428/211), Estonian Ministry of Education and Research (institutional research
571 funding project IUT8-2), and the Academy of Finland (Grant No. 266321).
572
573 REFERENCES
574
575 Alho, J. S., C. Matsuba, and J. Merilä, 2010 Sex reversal and primary sex ratios in
576 the common frog (*Rana temporaria*). Mol. Ecol. 19 (9): 1763-1773.
577 Bachtrog, D., 2013 Y-chromosome evolution: emerging insights into processes of
578 Y-chromosome degeneration. Nature Reviews Genetics 14 (2): 113-124.

579 Bernstein, B. E., M. Kamal, K. Lindblad-Toh, S. Bekiranov, D. K. Bailey *et al.*, 2005
580 Genomic maps and comparative analysis of histone modifications in
581 human and mouse. Cell 120 (2): 169-181.
582 Berset-Brändli, L., J. Jaquiéry, T. Broquet, Y. Ulrich, and N. Perrin, 2008 Extreme
583 heterochiasmy and nascent sex chromosomes in European tree frogs.
584 Proceedings of the Royal Society of London B: Biological Sciences 275
585 (1642): 1577-1585.
586 Brelsford, A., C. Dufresnes, and N. Perrin, 2016a High-density sex-specific linkage
587 maps of a European tree frog (*Hyla arborea*) identify the sex chromosome
588 without information on offspring sex. Heredity 116 (2): 177-181.
589 Brelsford, A., N. Rodrigues, and N. Perrin, 2016b High‐density linkage maps fail
590 to detect any genetic component to sex determination in a *Rana*
591 *temporaria* family. J. Evol. Biol. 29 (1): 220-225.
592 Brelsford, A., M. Stöck, C. Betto‐Colliard, S. Dubey, C. Dufresnes *et al.*, 2013
593 Homologous sex chromosomes in three deeply divergent anuran species.
594 Evolution 67 (8): 2434-2440.
595 Bruneaux, M., S. E. Johnston, G. Herczeg, J. Merilä, C. R. Primmer *et al.*, 2013
596 Molecular evolutionary and population genomic analysis of the nine‐
597 spined stickleback using a modified restriction‐site‐associated DNA
598 tag approach. Mol. Ecol. 22 (3): 565-582.
599 Cano, J. M., A. Laurila, J. Palo, and J. Merilä, 2004 Population differentiation in G
600 matrix structure due to natural selection in *Rana temporaria*. Evolution
601 58 (9): 2013-2020.

602 Cano, J. M., M.-H. Li, A. Laurila, J. Vilkki, and J. Merilä, 2011 First-generation
603 linkage map for the common frog *Rana temporaria* reveals sex-linkage
604 group. Heredity 107 (6): 530-536.
605 Carbone, L., S. G. Nergadze, E. Magnani, D. Misceo, M. F. Cardone *et al.*, 2006
606 Evolutionary movement of centromeres in horse, donkey, and zebra.
607 Genomics 87 (6): 777-782.
608 Cervera, M.-T., V. Storme, B. Ivens, J. Gusmao, B. H. Liu *et al.*, 2001 Dense genetic
609 linkage maps of three *Populus* species (*Populus deltoides*, *P. nigra* and *P.*
610 *trichocarpa*) based on AFLP and microsatellite markers. Genetics 158 (2):
611 787-809.
612 Chakravarti, A., L. K. Lasher, and J. E. Reefer, 1991 A maximum likelihood method
613 for estimating genome length using genetic linkage data. Genetics 128 (1):
614 175-182.
615 Charlesworth, B., and D. Charlesworth, 2000 The degeneration of Y
616 chromosomes. Philosophical Transactions of the Royal Society B:
617 Biological Sciences 355 (1403): 1563-1572.
618 Charlesworth, D., B. Charlesworth, and G. Marais, 2005 Steps in the evolution of
619 heteromorphic sex chromosomes. Heredity 95 (2): 118-128.
620 Chevreux, B., 2007 MIRA: an automated genome and EST assembler.
621 DaCosta, J. M., and M. D. Sorenson, 2014 Amplification biases and consistent
622 recovery of loci in a double-digest RAD-seq protocol. PloS one 9 (9):
623 e106713.
624 Doucleff, M., Y. Jin, F. Gao, S. Riaz, A. F. Krivanek *et al.*, 2004 A genetic linkage map
625 of grape, utilizing *Vitis rupestris* and *Vitis arizonica*. Theor. Appl. Genet.
626 109 (6): 1178-1187.

627 Duellman, W. E., and L. Trueb, 1986 *Biology of amphibians*. JHU press.
628 Dufresnes, C., M. Stöck, A. Brelsford, and N. Perrin, 2014 Range-wide sex-
629 chromosome sequence similarity supports occasional XY recombination
630 in European tree frogs (*Hyla arborea*). PloS one 9 (6): e97959.
631 Elshire, R. J., J. C. Glaubitz, Q. Sun, J. A. Poland, K. Kawamoto *et al.*, 2011 A robust,
632 simple genotyping-by-sequencing (GBS) approach for high diversity
633 species. PloS one 6 (5): e19379.
634 Fishman, L., A. J. Kelly, E. Morgan, and J. H. Willis, 2001 A genetic map in the
635 Mimulus guttatus species complex reveals transmission ratio distortion
636 due to heterospecific interactions. Genetics 159 (4): 1701-1716.
637 Gadau, J., C. U. Gerloff, N. Krüger, H. Chan, P. Schmid‐Hempel *et al.*, 2001 A
638 linkage analysis of sex determination in *Bombus terrestris*
639 (L.)(Hymenoptera: Apidae). Heredity 87 (2): 234-242.
640 Gagnaire, P. A., E. Normandeau, S. A. Pavey, and L. Bernatchez, 2013 Mapping
641 phenotypic, expression and transmission ratio distortion QTL using RAD
642 markers in the Lake Whitefish (*Coregonus clupeaformis*). Mol. Ecol. 22
643 (11): 3036-3048.
644 Gordon, A., and G. J. Hannon, 2010 Fastx-toolkit. FASTQ/A short-reads pre-
645 processing tools, Unpublished.
646 Green, D. M., and S. K. Sessions, 1991 *Amphibian cytogenetics and evolution*.
647 Academic Press, San Diego, California.
648 Hackett, C. A., and L. B. Broadfoot, 2003 Effects of genotyping errors, missing
649 values and segregation distortion in molecular marker data on the
650 construction of linkage maps. Heredity 90 (1): 33-38.

651 King, M., 1991 The evolution of heterochromatin in the amphibian genome, pp.
652 359-391 in *Amphibian cytogenetics and evolution*, edited by D. M. Green
653 and S. K. Sessions. Academic Press, San Diego, California.
654 Kocher, T. D., 2004 Adaptive evolution and explosive speciation: the cichlid fish
655 model. Nature Reviews Genetics 5 (4): 288-298.
656 Koonin, E. V., L. Aravind, and A. S. Kondrashov, 2000 The impact of comparative
657 genomics on our understanding of evolution. Cell 101 (6): 573-576.
658 Krzywinski, M., J. Schein, I. Birol, J. Connors, R. Gascoyne *et al.*, 2009 Circos: an
659 information aesthetic for comparative genomics. Genome Res. 19 (9):
660 1639-1645.
661 Kuittinen, H., A. A. de Haan, C. Vogl, S. Oikarinen, J. Leppälä *et al.*, 2004
662 Comparing the linkage maps of the close relatives *Arabidopsis lyrata* and
663 *A. thaliana*. Genetics 168 (3): 1575-1584.
664 Langmead, B., and S. L. Salzberg, 2012 Fast gapped-read alignment with Bowtie
665 2. Nat. Methods 9 (4): 357-359.
666 Laugen, A. T., A. Laurila, K. Räsänen, and J. Merilä, 2003 Latitudinal
667 countergradient variation in the common frog (*Rana temporaria*)
668 development rates – evidence for local adaptation. J. Evol. Biol. 16 (5):
669 996-1005.
670 Laurila, A., S. Karttunen, and J. Merilä, 2002 Adaptive phenotypic plasticity and
671 genetics of larval life histories in two *Rana temporaria* populations.
672 Evolution 56 (3): 617-627.
673 Lee, C. E., 2002 Evolutionary genetics of invasive species. Trends Ecol. Evol. 17
674 (8): 386-391.

675 Li, H., B. Handsaker, A. Wysoker, T. Fennell, J. Ruan *et al.*, 2009 The sequence
676 alignment/map format and SAMtools. Bioinformatics 25 (16): 2078-2079.
677 Li, W., 2015 Fast Program for Clustering and Comparing Large Sets of Protein or
678 Nucleotide Sequences, pp. 173-177 in *Encyclopedia of Metagenomics*.
679 Springer.
680 Lyttle, T. W., 1991 Segregation distorters. Annu. Rev. Genet. 25 (1): 511-581.
681 Matsuba, C., I. Miura, and J. Merilä, 2008 Disentangling genetic vs. environmental
682 causes of sex determination in the common frog, *Rana temporaria*. BMC
683 Genet. 9 (1): 3.
684 Miaud, C., R. Guyétant, and J. Elmberg, 1999 Variations in life-history traits in the
685 common frog *Rana temporaria* (Amphibia: Anura): a literature review and
686 new data from the French Alps. J. Zool. 249 (01): 61-73.
687 Miller, M. R., J. P. Dunham, A. Amores, W. A. Cresko, and E. A. Johnson, 2007 Rapid
688 and cost-effective polymorphism identification and genotyping using
689 restriction site associated DNA (RAD) markers. Genome Res. 17 (2): 240-
690 248.
691 Morescalchi, A., and M. Galgano, 1973 Meiotic chromosomes and their taxonomic
692 value in Amphibia Anura. Caldasia: 41-50.
693 Nadeau, N. J., and C. D. Jiggins, 2010 A golden age for evolutionary genetics?
694 Genomic studies of adaptation in natural populations. Trends Genet. 26
695 (11): 484-492.
696 Ozerov, M. Y., R. Gross, M. Bruneaux, J. P. Vähä, O. Burimski *et al.*, 2016 Genome‐
697 wide introgressive hybridization patterns in wild Atlantic salmon
698 influenced by inadvertent gene flow from hatchery releases. Mol. Ecol. 25:
699 1275-1290.

700 Palo, J. U., D. S. Schmeller, A. Laurila, C. R. Primmer, S. L. Kuzmin *et al.*, 2004 High
701 degree of population subdivision in a widespread amphibian. Mol. Ecol.
702 13 (9): 2631-2644.
703 Perrin, N., 2009 Sex reversal: a fountain of youth for sex chromosomes?
704 Evolution 63 (12): 3043-3049.
705 Phillimore, A. B., J. D. Hadfield, O. R. Jones, and R. J. Smithers, 2010 Differences in
706 spawning date between populations of common frog reveal local
707 adaptation. Proc Natl Acad Sci U S A 107 (18): 8292-8297.
708 Pukk, L., F. Ahmad, S. Hasan, V. Kisand, R. Gross *et al.*, 2015 Less is more: extreme
709 genome complexity reduction with ddRAD using Ion Torrent
710 semiconductor technology. Mol. Ecol. Resour. 15 (5): 1145-1152.
711 Pyron, R. A., and J. J. Wiens, 2011 A large-scale phylogeny of Amphibia including
712 over 2800 species, and a revised classification of extant frogs,
713 salamanders, and caecilians. Mol. Phylogen. Evol. 61 (2): 543-583.
714 R Core Team, 2013 R Foundation for Statistical Computing. Vienna, Austria 3 (0).
715 Rodrigues, N., C. Betto‐Colliard, H. Jourdan‐Pineau, and N. Perrin, 2013
716 Within‐population polymorphism of sex‐determination systems in the
717 common frog (*Rana temporaria*). J. Evol. Biol. 26 (7): 1569-1577.
718 Rodrigues, N., J. Merilä, C. Patrelle, and N. Perrin, 2014 Geographic variation in
719 sex‐chromosome differentiation in the common frog (*Rana temporaria*).
720 Mol. Ecol. 23 (14): 3409-3418.
721 Rodrigues, N., Y. Vuille, A. Brelsford, J. Merilä, and N. Perrin, 2016 The genetic
722 contribution to sex determination and number of sex chromosomes vary

among populations of common frogs (*Rana temporaria*). Heredity 117 (1): 25-32.

Rogers, S. M., N. Isabel, and L. Bernatchez, 2007 Linkage maps of the dwarf and normal lake whitefish (*Coregonus clupeaformis*) species complex and their hybrids reveal the genetic architecture of population divergence. Genetics 175 (1): 375-398.

Schmeller, D. S., J. U. Palo, and J. Merilä, 2008 A contact zone between two distinct *Rana temporaria* lineages in northern Germany. Alytes 25 (3-4): 93-98.

Seoane, V. L., 1885 On two forms of *Rana* from NW Spain. The zoologist 9: 169-172.

Spasić-Bošković, O., N. Tanić, J. Blagojević, and M. Vujošević, 1997 Comparative cytogenetic analysis of European brown frogs: *Rana temporaria*, *R. dalmatina* and *R. graeca*. Caryologia 50 (2): 139-149.

Stöck, M., R. Savary, C. Betto‐Colliard, S. Biollay, H. Jourdan‐Pineau *et al.*, 2013 Low rates of X‐Y recombination, not turnovers, account for homomorphic sex chromosomes in several diploid species of Palearctic green toads (*Bufo viridis* subgroup). J. Evol. Biol. 26 (3): 674-682.

Taylor, D. R., and P. K. Ingvarsson, 2003 Common features of segregation distortion in plants and animals. Genetica 117 (1): 27-35.

Teacher, A. G. F., T. W. J. Garner, and R. A. Nichols, 2009 European phylogeography of the common frog (*Rana temporaria*): routes of postglacial colonization into the British Isles, and evidence for an Irish glacial refugium. Heredity 102 (5): 490-496.

Van Ooijen, J. W., 2011 Multipoint maximum likelihood mapping in a full-sib family of an outbreeding species. Genetics research 93 (05): 343-349.

748 Veith, M., J. Kosuch, and M. Vences, 2003 Climatic oscillations triggered post-
749 Messinian speciation of Western Palearctic brown frogs (Amphibia,
750 Ranidae). Mol. Phylogen. Evol. 26 (2): 310-327.
751 Veith, M., M. Vences, D. R. Vieites, S. Nieto-Roman, and A. Palanca, 2002 Genetic
752 differentiation and population structure within Spanish common frogs
753 (*Rana temporaria* complex; Ranidae, Amphibia). Folia zoologica-praha- 51
754 (4): 307-318.
755 Vences, M., J. S. Hauswaldt, S. Steinfartz, O. Rupp, A. Goesmann *et al.*, 2013
756 Radically different phylogeographies and patterns of genetic variation in
757 two European brown frogs, genus *Rana*. Mol. Phylogen. Evol. 68 (3): 657-
758 670.
759 Vilstrup, J. T., A. Seguin-Orlando, M. Stiller, A. Ginolhac, M. Raghavan *et al.*, 2013
760 Mitochondrial phylogenomics of modern and ancient equids. PLoS One 8
761 (2): e55950.
762 Wu, Y., P. R. Bhat, T. J. Close, and S. Lonardi, 2008 Efficient and accurate
763 construction of genetic linkage maps from the minimum spanning tree of
764 a graph. PLoS Genet. 4 (10): e1000212.
765 Yang, L., D. H. Koo, D. Li, T. Zhang, J. Jiang *et al.*, 2014 Next‐generation
766 sequencing, FISH mapping and synteny‐based modeling reveal
767 mechanisms of decreasing dysploidy in Cucumis. The Plant Journal 77 (1):
768 16-30.
769 Zhou, W., Z. Tang, J. Hou, N. Hu, and T. Yin, 2015 Genetic map construction and
770 detection of genetic loci underlying segregation distortion in an
771 intraspecific cross of *Populus deltoides*. PloS one 10 (5): e0126077.
772

773

774 Labels:

775

776 Table 1: Linkage group length, total number of markers, recombination rate and

777 number of markers in the non-recombining region by sex.

778

779 Figure 1: Difference in recombination between sexes. While the female map

780 shows a more uniform recombination rate across all linkage groups, the male

781 map exhibits non-recombining regions as peaks of high marker density.

782

783 Figure 2: Female vs. male number of markers for each linkage group.

784

785 Figure 3. Circos plot showing the strong synteny between *Xenopus tropicalis* and

786 *Rana temporaria*. To obtain a better visualization, the number of base pairs of the

787 *R. temporaria* linkage groups was multiplied by 100.

788

LG	Length (cM)		N markers		Recombination rate		N markers within cold spot	
	Male	Female	Male	Female	Male	Female	Male	Female
Rt1	392.838	914.948	551	631	0.71	1.45	108	8
Rt2	323.074	778.775	435	497	0.74	1.57	159	13
Rt3	239.262	694.948	383	453	0.62	1.53	117	16
Rt4A	199.211	304.537	178	160	1.12	1.9	52	9
Rt4B	212.494	259.109	114	161	1.86	1.61	22	22
Rt5	265.076	664.933	323	481	0.82	1.38	86	7
Rt6	362.237	597.954	422	339	0.86	1.76	150	10
Rt7A	205.762	295.579	144	177	1.43	1.67	19	8
Rt7B	119.879	218.716	70	125	1.71	1.75	9	9
Rt8A	149.881	209.416	85	96	1.76	2.18	15	4
Rt8B	159.626	273.802	135	158	1.18	1.73	62	6
Rt9	200.646	277.64	133	173	1.51	1.6	28	12
Rt10	222.21	217.664	132	145	1.68	1.5	16	17
TOT	**3052.196**	**5708.021**	**3105**	**3596**	**1.23**	**1.67**	**-**	**-**

789

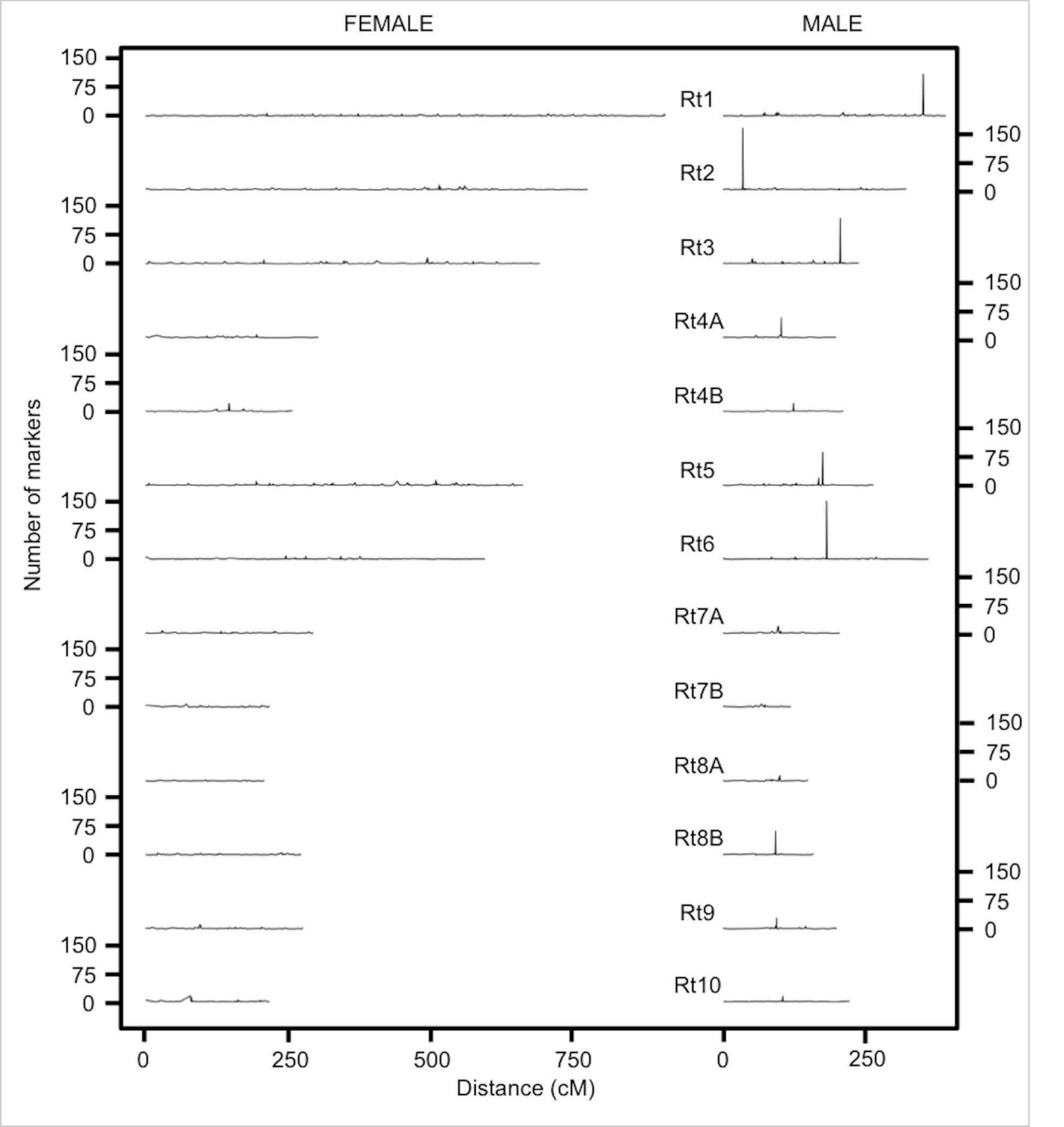
FEMALE
MALE
Number of markers
Distance (cM)
Rt1
Rt2
Rt3
Rt4A
Rt4B
Rt5
Rt6
Rt7A
Rt7B
Rt8A
Rt8B
Rt9
Rt10
150
75
0
0
250
500
750

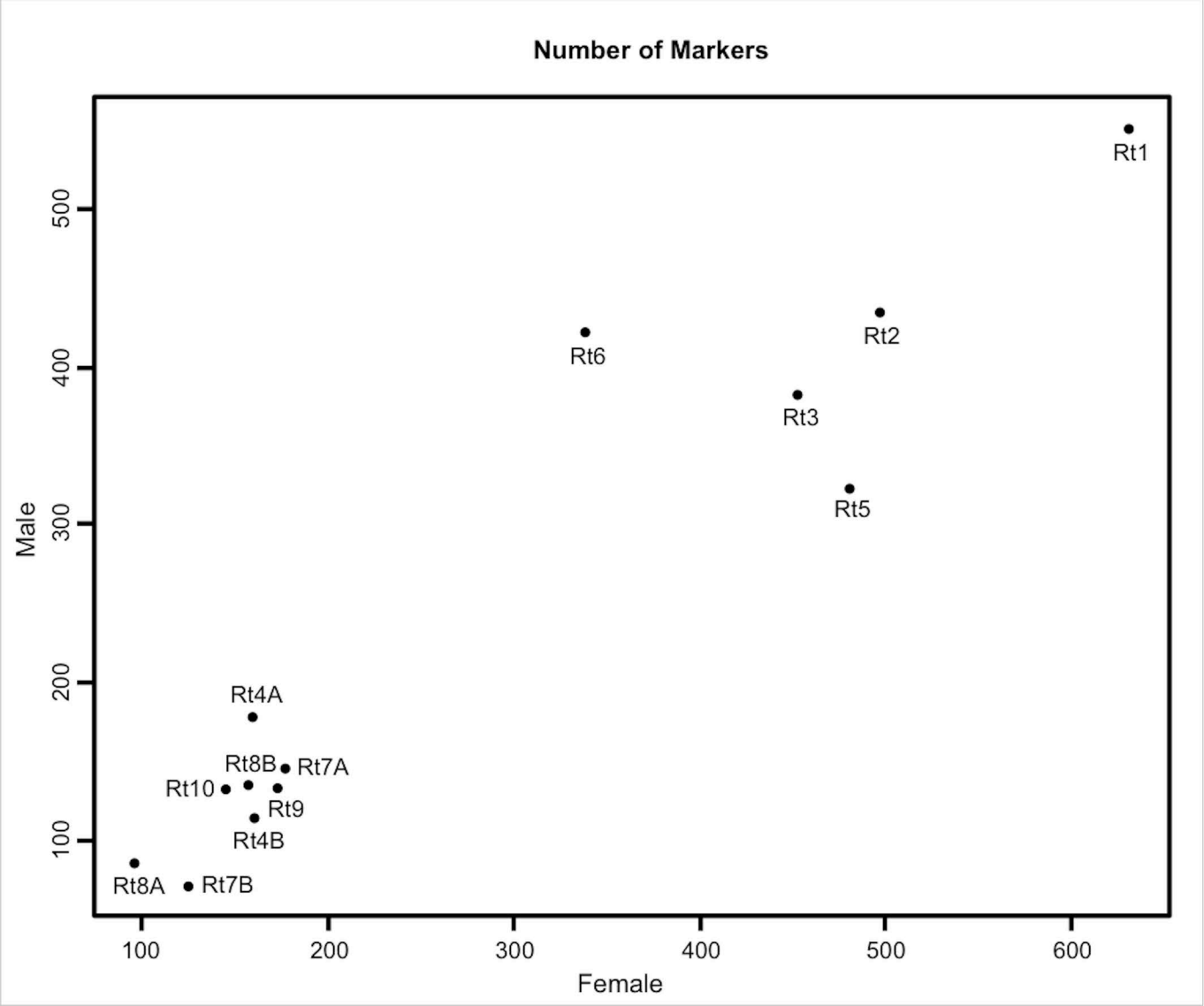
Number of Markers
Male
Female
100
200
300
400
500
600
Rt1
Rt2
Rt3
Rt4A
Rt4B
Rt5
Rt6
Rt7A
Rt7B
Rt8A
Rt8B
Rt9
Rt10

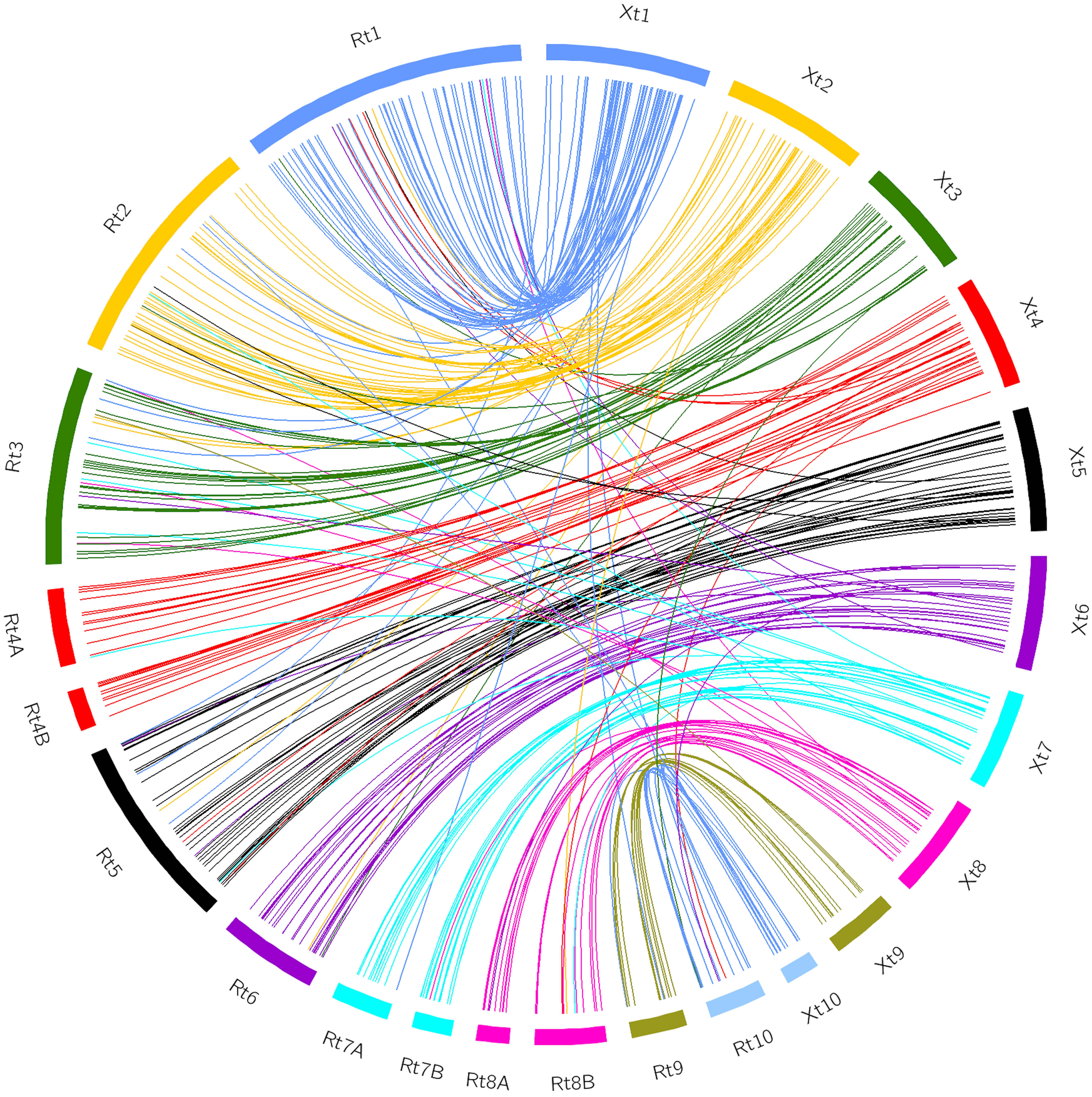
Xt1
Xt2
Xt3
Xt4
Xt5
Xt6
Xt7
Xt8
Xt9
Xt10
Rt1
Rt2
Rt3
Rt4A
Rt4B
Rt5
Rt6
Rt7A
Rt7B
Rt8A
Rt8B
Rt9
Rt10